The mechanism for polarity inversion of GaN via a thin AlN layer: Direct experimental evidence

Fude Liu,[a] Ramon Collazo, Seiji Mita, Zlatko Sitar, and Gerd Duscher[b]
Department of Materials Science and Engineering, North Carolina State University, Raleigh, North Carolina 27606, USA

Stephen J. Pennycook
Materials Science and Technology Division, Oak Ridge National Laboratory, Oak Ridge, Tennessee 37831, USA

(Received 16 October 2007; accepted 30 October 2007; published online 15 November 2007)

Lateral-polarity heterostructures of GaN on *c* sapphire were prepared by deposition and patterning of a thin low-temperature AlN nucleation layer. Adjacent macroscopic domains were found to have opposite polarity; domains grown on the AlN nucleation layer were Ga polar while those grown on the nitrided sapphire were N polar, as confirmed by convergent-beam electron diffraction and *Z*-contrast images. We directly determined the atomic interface structure between the AlN and *c* sapphire with an aberration-corrected scanning transmission electron microscope at ~1.0 Å resolution. This is the direct experimental evidence for the origin of the polarity control in III nitrides. This understanding is an important step toward manipulating polarity in these semiconductors. © *2007 American Institute of Physics*. [DOI: 10.1063/1.2815748]

Wide-bandgap III nitrides play an important role in modern devices.[1–3] Compared to Si and SiC, sapphire offers a compromise as the most widely used substrate material for III-nitride growth to date. Moreover, the crystal polarity of GaN can be easily controlled: N-polar films are obtained when GaN is directly grown on nitrided sapphire and Ga polar when GaN is grown on sapphire coated with a thin low-temperature (LT)-AlN layer.[4] This ability provides an additional degree of freedom for control of properties in III nitrides and potential for devices.[5–7] A particularly interesting possibility, which uses the polarity of GaN, is the growth of lateral-polarity heterostructures with predetermined macroscopic domains of different polarities separated by inversion domain boundaries (IDBs) (Fig. 1)[5,7] However, no direct, indisputable determination of the interface structures (including the interface between GaN and sapphire) has yet been made, which would aid understanding of the mechanism for polarity control.

The films were grown by a "two-step" metal-organic vapor-phase epitaxy process with a thermal cleaning at 1070 °C in flowing H_2 and nitridation at 935 °C of the *c*-sapphire substrate; a 30 nm LT-AlN nucleation layer was then grown at 600 °C. The LT-AlN layer was patterned with photolithography and etching. A ~1-μm-thick GaN film was subsequently grown on the patterned and nitrided sapphire at a higher temperature of 1030 °C so that lateral-polarity heterostructures consisting of Ga-polar and N-polar domains were achieved side-by-side on a single sapphire wafer. Nitrogen was used as dilution and carrier gas throughout the growth process, which was under the mass-transport-limited growth regime. The details of the growth process have been presented elsewhere.[8] Transmission electron microscopy (TEM) specimens were prepared by the standard mechanical-grinding and ion-milling methods. *Z*-contrast images were taken with a VG Microscopes HB-501UX 100 kV scanning TEM (STEM) at Oak Ridge National Laboratory fitted with a Nion aberration corrector, giving an expected probe size in the range of 1.0 Å. The images were low-pass filtered to reduce the noise using Gatan DigitalMicrograph software. Convergent-beam electron diffraction (CBED) patterns were acquired with a JEOL2010F TEM/STEM operated at 200 kV at North Carolina State University. CBED simulations were carried out with electron microscopy software (JAVA version),[9] using the Bloch-wave approach.

Figure 1 shows the two widely cited IDB models.[10,11] On the left side, the GaN lattice is N polar, the crystallographic *c* axis and internal electric field *E* point toward the interface with the substrate, and the macroscopic polarization *P* points toward the surface. On the right side, the directions are inverted. The two kinds of IDBs are on the $(0\bar{1}10)$ and $(\bar{2}110)$

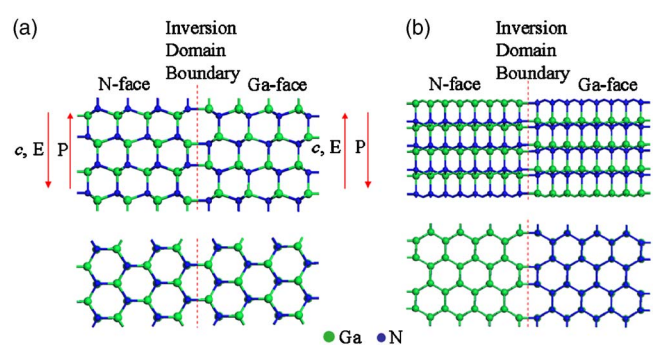

FIG. 1. (Color online) Schematic of two theoretical GaN IDB models.(a) Cross-sectional view (top) in the $[\bar{2}110]$ projection and its corresponding top-down view (bottom), where the IDB is on the $(0\bar{1}10)$ plane. The polarization *P*, crystallographic *c* axis, and internal electric field *E* are indicated by red arrows. The same is true for the second model shown in (b). (b) Cross-sectional view (top) in the $[0\bar{1}10]$ projection and its corresponding top-down view (bottom), where the IDB is on the $(\bar{2}110)$ plane.

[a]Author to whom correspondence should be addressed. Present address: MailStop 3215, National Center for Photovoltaics, National Renewable Energy Laboratory, Golden, CO 80401. Tel.: 303-384-7677. FAX: 303-384-6490. Electronic mail: fude_liu@nrel.gov
[b]Also at Materials Science and Technology Division, Oak Ridge National Laboratory, Oak Ridge, TN 37831, USA.

 © 2007 American Institute of Physics
Downloaded 18 Aug 2008 to 160.91.172.37. Redistribution subject to AIP license or copyright; see http://apl.aip.org/apl/copyright.jsp

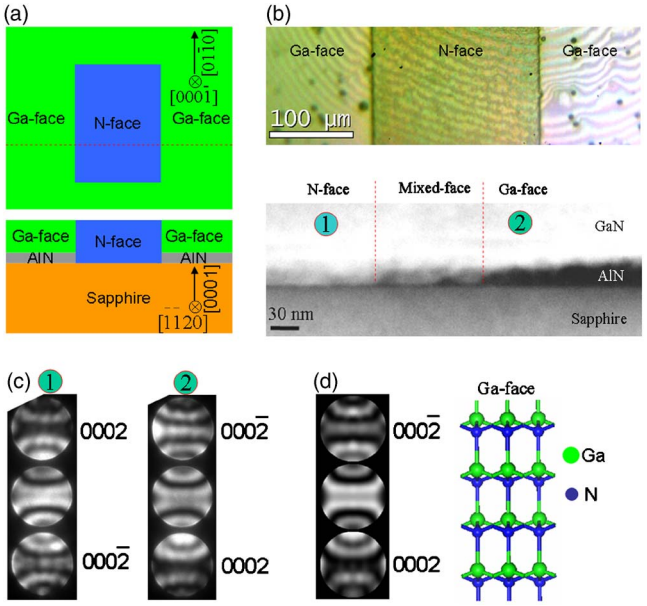

FIG. 2. (Color online) Lateral-polarity heterostructures. (a) Schematic of the heterostructures, including the top-down view (top) and the cross-sectional view (bottom). The red dashed line corresponds to the cross section. (b) Corresponding optical microscopy image (top-down view) and *Z*-contrast image (cross-sectional view in the $[0\bar{1}10]$ projection) of the heterostructures. 1 and 2 represent two positions where the CBED patterns were acquired. (c) Two CBED patterns show the opposite polarity of position 1 and 2. (d) Simulated CBED pattern, where the $[0\bar{1}10]$ zone axis was applied and the specimen thickness was set at 104 nm, and schematic of the corresponding GaN lattice in this projection.

planes, respectively, which are perpendicular to each other (they can also form an angle of 30° if we consider equivalent planes; in this work, we considered only the former case). We therefore prepared the lateral-polarity heterostructures, with the end edges of the LT-AlN layer along the $[\bar{2}110]$ and $[0\bar{1}10]$ directions to achieve the two kinds of IDBs, respectively.

Figure 2(a) schematically shows the heterostructures, including the top-down view (top) and the cross-sectional view (bottom). The corresponding optical microscopy image (top-down view) and *Z*-contrast image (cross-sectional view in the $[0\bar{1}10]$ projection) are shown in Fig. 2(b). To determine the relative polarity of GaN on both sides of IDBs, we carried out CBED. The zone axis $[0\bar{1}10]$ was chosen because of the clearer CBED pattern features, compared with the patterns obtained on the $[\bar{2}110]$ zone axis. The CBED patterns indicate that the positions "1" and "2" have opposite polarity, as seen from the different contrasts in the 0002 and $000\bar{2}$ disks due to the strong dynamical effect of electron diffraction [Fig. 2(c)]. Also, the detected regions have a thickness of ~104 nm by matching the experimentally obtained CBED patterns with Bloch-wave simulations [Fig. 2(d)].

Z-contrast images of the interface between the LT-AlN nucleation layer and *c* sapphire are shown in Fig. 3. In a *Z*-contrast image, only large-angle Rutherford scattered electrons are collected with an annular dark-field detector, causing its image intensity to be approximately proportional to Z^2 (Z is the average atomic number).[12] Therefore, AlN appears darker than sapphire in a *Z*-contrast image. The inset is the reconstructed image after selected Fourier filtering to reveal the misfit edge dislocations at the interface, caused by

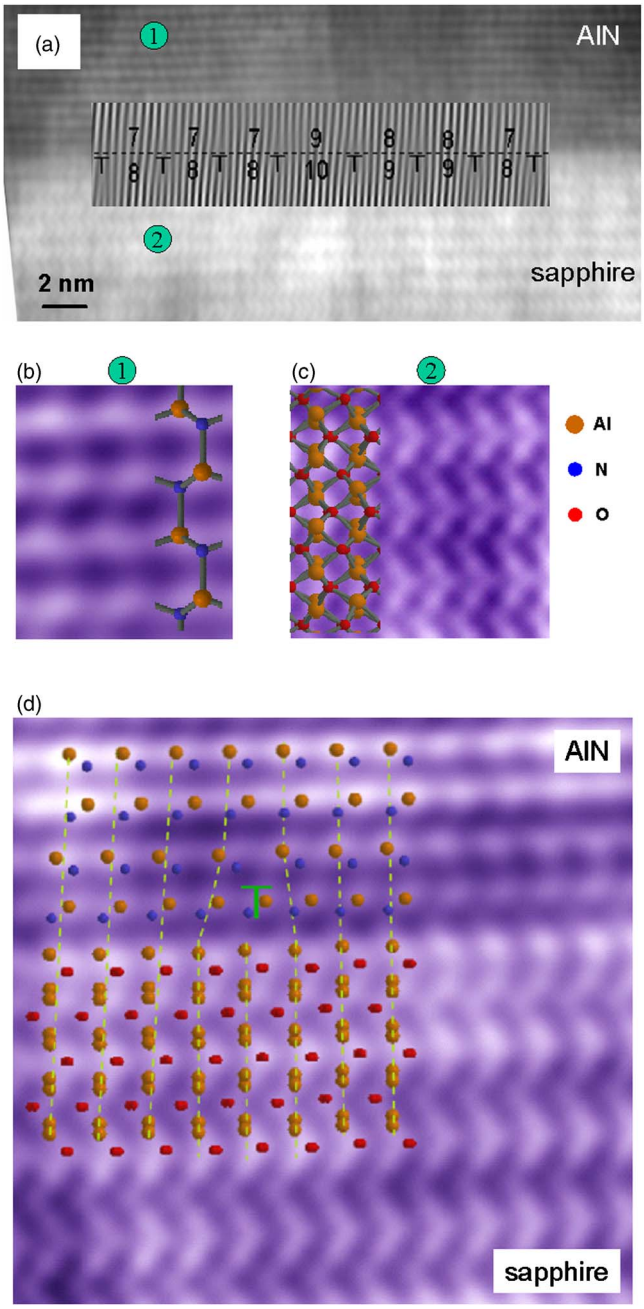

FIG. 3. (Color online) *Z*-contrast images in the $[\bar{2}110]$ projection of AlN. (a) Low-magnification *Z*-contrast image. The inset is the reconstructed image after selected Fourier filtering to reveal the 8.5:7.5 misfit edge dislocations. The numbers indicate the positions where the atomic-resolution *Z*-contrast images were taken. (b) Atomic-resolution *Z*-contrast image of AlN taken from position 1. (c) Atomic-resolution Z-contrast image of sapphire taken from position 2. (d) Atomic-resolution *Z*-contrast image of the interface and its atomic fitting model in the $[\bar{2}110]$ projection of AlN. The green "T" indicates the misfit edge dislocation.

the large lattice mismatch between AlN and sapphire (13.29% in *c* plane). In the $[\bar{2}110]$ projection of AlN, the Al–Al distance in the $[01\bar{1}0]$ direction is 2.695 Å, while in the $[\bar{1}100]$ projection of sapphire, the Al–Al distance in the $[11\bar{2}0]$ direction is 2.379 Å. The Al–Al distance difference means that about every 7.5 Al–Al distances in AlN correspond to about 8.5 Al–Al distances in sapphire [Fig. 3(a)]. The experimental ratio was determined to be 7.7:8.7, which is close to the theoretical value of 7.5:8.5. This result is

Downloaded 18 Aug 2008 to 160.91.172.37. Redistribution subject to AIP license or copyright; see http://apl.aip.org/apl/copyright.jsp

consistent with that mentioned in Ref. 13. Before determining the atomic interface structure, it is important to know the polarity of AlN and the complicated lattice structure of sapphire. So far, a few methods have been used to identify the polarity of hexagonal III nitrides such as chemical etching,[14] CBED,[15] and ultraviolet-photoelectron emission microscopy.[16] Figure 3(b) shows the atomic-resolution *Z*-contrast image taken at position 1 from AlN. In this figure, the N columns are seen as elongations of the Al column images alternately pointing diagonally left and right. From this, one can directly determine that AlN is in this case Al polar and GaN grown upon it should have Ga polarity. The direct polarity determination of AlN was realized only recently.[17] The lattice structure of sapphire has been well known for a long time.[18] However, the complicated lattice structure of sapphire has made direct atomic imaging extremely challenging. Direct imaging of a crystal lattice has been realized recently with high-resolution aberration-corrected STEM *Z*-contrast imaging.[19] As shown in Fig. 3(c), we are able to determine directly the lattice structure of sapphire with this method since the columns of O and Al are arranged in a zigzag pattern in this projection.

The atomic-resolution *Z*-contrast image of the interface is shown in Fig. 3(d), where the atomic model fits the experimentally obtained structure well. Note that there are a few interesting results. The lattice-misfit edge dislocation is observed, as expected before. However, the dislocation plane is not the interface plane, but is one Al–N monolayer above the interface. This monolayer acts as a transition layer to tolerate the lattice mismatch between AlN and sapphire. Usually, "epiready" sapphire substrates are oxygen terminated after nitridation.[5] Actually, it should not matter in this case whether the substrate is oxygen terminated or Al terminated. As seen from the *Z*-contrast image, it clearly shows that the top Al monolayer on sapphire follows the sapphire bulk structure and then belongs to sapphire but not to AlN, which determined the III-polar polarity. This is reasonable, because Al–O bonds are stronger than Al–N bonds.[20] Therefore, this result represents the direct experimental evidence as to why a proper AlN nucleation layer enables growth of Ga-polar GaN films.

These findings are consistent with our early results reported elsewhere,[8,21] which are summarized in Fig. 4. The flow chart shows the experimental observations on the polarity selection of GaN when different processing conditions are applied. As shown in Fig. 4, GaN is Ga polar when a thin AlN layer is applied while it is N polar when directly grown on nitrided sapphire.

In summary, we prepared lateral-polarity heterostructures of GaN on *c* sapphire, where the adjacent predetermined macroscopic domains were found to have opposite polarity using CBED. We directly determined the interface structure of AlN on *c* sapphire at angstrom resolution. This is the direct experimental evidence for the origin of the polarity control of GaN via a thin LT-AlN layer. This understanding is an important step toward manipulating the polarity in III-nitride semiconductors.

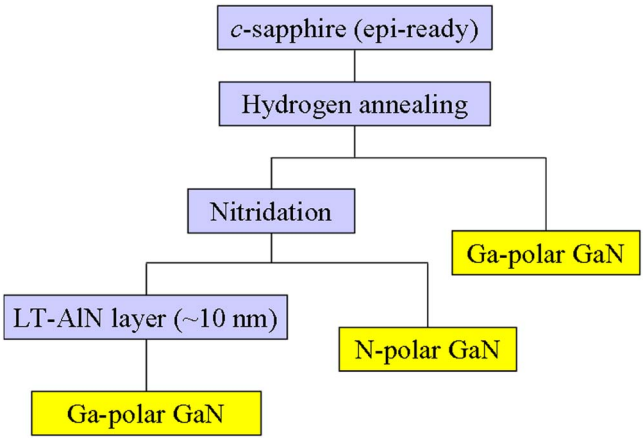

FIG. 4. (Color online) Flow chart of experimental observations on the polarity selection of GaN under different processing conditions.

This work was funded by the Office of Naval Research under Contract No. N00014-01-1-0716, with Dr. Colin Wood, project monitor, and by the Division of Materials Science and Engineering (S.J.P.), U.S. Department of Energy.

[1] L. F. Eastman and U. K. Mishra, IEEE Spectrum **39**, 28 (2002).
[2] Y. Taniyasu, M. Kasu, and T. Makimoto, Nature (London) **441**, 325 (2006).
[3] S. A. Wolf, D. D. Awschalom, R. A. Buhrman, J. M. Daughton, S. V. Molnár, M. L. Roukes, A. Y. Chtchelkanova, and D. M. Treger, Science **294**, 1448 (2001).
[4] R. Collazo, S. Mita, R. Schlesser, and Z. Sitar, Phys. Status Solidi C **2**, 2117 (2005).
[5] M. Stutzmann, O. Ambacher, M. Eickhoff, U. Karrer, A. L. Pimenta, R. Neuberger, J. Schalwig, R. Dimitrov, P. J. Schuck, and R. D. Grober, Phys. Status Solidi B **228**, 505 (2001).
[6] M. Sumiya and S. Fuke, MRS Internet J. Nitride Semicond. Res. **9**, 1 (2004).
[7] P. J. Schuck, M. D. Mason, R. D. Grober, O. Ambacher, A. P. Lima, C. Miskys, R. Dimitrov, and M. Stutzmann, Appl. Phys. Lett. **79**, 952 (2001).
[8] R. Collazo, S. Mita, A. Aleksov, R. Schlesser, and Z. Sitar, J. Cryst. Growth **287**, 586 (2006).
[9] P. Stadelmann, Electron Microscopy Software (Java Version 1.3422W2003), CIME-EPFL, Switzerland, 1999–2003.
[10] J. E. Northrup, J. Neugebauer, and L. T. Romano, Phys. Rev. Lett. **77**, 103 (1996).
[11] J. E. Northrup, Physica B **273-274**, 130 (1999).
[12] R. F. Egerton, *Physical Principles of Electron Microscopy* (Springer, New York, 2005), p. 177.
[13] *Optoelectronic Devices: III-Nitrides*, edited by M. Razeghi and M. Henini (Elsevier, Amsterdam, 2004), p. 251.
[14] H. M. Ng, W. Parz, N. G. Weimann, and A. Chowdhury, Jpn. J. Appl. Phys., Part 2 **42**, L1405 (2003).
[15] D. B. Williams and C. B. Carter, *Transmission Electron Microscopy: a Textbook for Materials Science* (Plenum, New York, 1996), Vol. 2, p. 339.
[16] W.-C. Yang, B. J. Rodriguez, M. Park, R. J. Nemanich, O. Ambacher, and V. Cimalla, J. Appl. Phys. **94**, 5720 (2003).
[17] K. A. Mkhoyan, P. E. Batson, J. Cha, W. J. Schaff, and J. Silcox, Science **312**, 1354 (2006).
[18] I. Levin and D. Brandon, J. Am. Ceram. Soc. **81**, 1995 (1998).
[19] P. D. Nellist, M. F. Chisholm, N. Dellby, O. L. Krivanek, M. F. Murfitt, Z. S. Szilagyi, A. R. Lupini, A. Borisevich, W. H. S., Jr., and S. J. Pennycook, Science **305**, 1741 (2004).
[20] *CRC Handbook of Chemistry and Physics*, 84th edition, edited by D. R. Lide (CRC, Boca Raton, FL, 2003), p. 9.
[21] A. Aleksov, R. Collazo, S. Mita, R. Schlesser, and Z. Sitar, Appl. Phys. Lett. **89**, 052117 (2006).

Downloaded 18 Aug 2008 to 160.91.172.37. Redistribution subject to AIP license or copyright; see http://apl.aip.org/apl/copyright.jsp